C. R. Mecanique 347 (2019) 389–396

Contents lists available at ScienceDirect

Comptes Rendus Mecanique

www.sciencedirect.com

Extension of the lubrication theory for arbitrary wall shape: An asymptotic analysis

Rogers Bill Cordova Hinojosa, Kim Pham *, Corinne Rouby

IMSIA, CNRS, ENSTA ParisTech, 828, bd des Maréchaux, 91732 Palaiseau, France

ARTICLE INFO

Article history:
Received 23 January 2019
Accepted 27 March 2019
Available online 19 April 2019

Keywords:
Lubrication approximation
Stokes flow
Asymptotic expansions

ABSTRACT

We extend the lubrication approximation for a viscous flow in two-dimensional channels with arbitrary shape functions and moderate aspect ratio. The higher-order model is obtained following an asymptotic analysis. Velocity and pressure profiles for the approximated model are given analytically and involve the derivatives of the shape functions of the walls up to the second order. Comparisons with full-scale simulations are given and show good agreement as well as improvements from the classical standard lubrication approximation.

1. Introduction

The *Classical Lubrication Approximation* (CLA) accounts for the behavior of viscous flows in thin channels under the assumption of small Reynolds numbers and for slowly varying walls. Under these hypotheses, the flow is characterized by (i) a constant pressure across the transverse, say vertical, section and with variations along the channel axis governed by the Reynolds equation [1], (ii) a horizontal velocity of the Poiseuille type and a vertical velocity negligible compared to the horizontal velocity.

The CLA, as it avoids us to resolve a full-scale fluid calculation, is used in many fields such as film lubricant [2], hydraulic fracture mechanics [3,4], dykes and sills in volcanism [5], or flows in biological systems such as blood cell transport in narrow capillaries [6]. However, its validity as that of the associated Reynolds equation have to be questioned when the curvature of the channel is not negligible anymore. A systematic way to do so is to use asymptotic techniques, which are well adapted due to the small thickness of the channel compared to the other dimensions. Starting in the 1980s, such an *Extended Lubrication Approximation* (ELA) has been applied to channels with a single wavy wall [7] and with two symmetric wavy walls [8]. In these references, power series of the stream function have been obtained for low Reynolds numbers and the results have been applied in hydraulic fracture mechanics, see, *e.g.*, [9] and references herein. We also mention the works of [10] concerning roughnesses for which the asymptotic analysis is combined with homogenization to extract the macroscopic effective behavior. Recently, Tavakol and co-workers have revisited the problem of a single wavy wall using a slightly different approach in which the asymptotic analysis is applied to the Stokes equations [11]. Experimental and numerical results support their analytical result and exemplify the interest of the improved model to capture accurately the velocity profiles and the pressure drop. Our study follows from this work and extends the lubrication approximation to two non-symmetric wavy walls.

* Corresponding author.
E-mail address: kim.pham@ensta-paristech.fr (K. Pham).

https://doi.org/10.1016/j.crme.2019.03.016

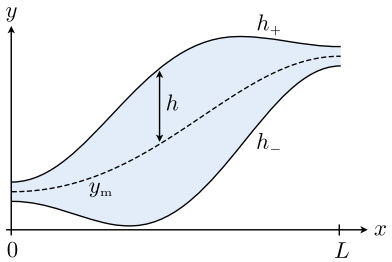

Fig. 1. Schematic view of a channel of length L with arbitrary upper and lower shape profiles $h_+(x)$ and $h_-(x)$. The functions $h(x)$ and $y_m(x)$ denote the half-distance between the walls and the average level, respectively.

The paper is organized as follows. The problem is introduced in Section 2 along with the main result of the paper. In Section 3, we will proceed to the derivation of ELA by means of asymptotic techniques. Finally, in Section 4, we compare the behavior of the second-order asymptotic approximation to direct numerical simulations and to the prediction from the standard lubrication theory.

2. Problem setting and main result

We consider an incompressible, steady, two-dimensional pressure-driven flow in a channel of length L. The geometry is defined through the introduction of the upper shape function $y = h_+(x)$ and the lower shape function $y = h_-(x)$ for $x \in (0, L)$ with $h_+ > h_-$ (see Fig. 1). These functions are assumed to be at least C^2 continuous. We introduce the mean line level y_m and the local half-thickness h of the channel defined by

$$y_m = \frac{h_+ + h_-}{2}, \qquad h = \frac{h_+ - h_-}{2} \tag{1}$$

both being function of x. We then rescale the vertical coordinate and center it around the average level according to

$$\mathrm{y} = \frac{y - y_m(x)}{h(x)} \tag{2}$$

The Reynolds number is assumed to be small, so that the flow is governed by the Stokes equations

$$\nabla \cdot \mathbf{u} = 0, \qquad \mu \nabla^2 \mathbf{u} = \nabla p \tag{3}$$

where $\mathbf{u} = u\mathbf{e}_x + v\mathbf{e}_y$ and p are the velocity and the pressure fields, respectively, and μ is the viscosity of the fluid. Additionally to a no-slip condition on the walls, the boundary conditions are defined as prescribed as a Poiseuille inlet velocity profile and a vanishing outlet pressure

$$\mathbf{u}(x, h_+(x)) = \mathbf{u}(x, h_-(x)) = \mathbf{0}, \qquad \mathbf{u}(0, y) = \frac{3\Phi}{4h(0)}\left(1 - \mathrm{y}^2\right)\mathbf{e}_x, \qquad p(L, y) = 0 \tag{4}$$

with Φ the fluid flux. To conduct the asymptotic analysis, we define the small parameter

$$\varepsilon = \frac{h(0)}{L} \tag{5}$$

which accounts for the slenderness ratio of the channel. The main result of the paper is the following approximation of the exact solution to the problem up to the second order in the small parameter ε

$$u(x, y) = \frac{3\Phi}{4h}\left(1 - \mathrm{y}^2\right)\left(1 + \frac{4h'^2 - hh''}{10}\left(1 - 5\mathrm{y}^2\right) + \frac{2hy_m'' - 12h'y_m'}{3}\,\mathrm{y}\right) + u_c o(\varepsilon^2) \tag{6}$$

$$v(x, y) = \frac{3\Phi}{4h}\left(1 - \mathrm{y}^2\right)\left(h'\mathrm{y} + y_m'\right) + u_c o(\varepsilon^2) \tag{7}$$

$$p(x, y) = \mu\Phi \int_x^L \frac{3}{2h^3}\left(1 + \frac{2}{5}\left(h'^2 + hh'' + 5y_m'^2\right)\right)\mathrm{d}x' + \frac{3\mu\Phi}{4h^2}\left(h'(1 - 3\mathrm{y}^2) - 2y_m'\mathrm{y}\right) + p_c o(\varepsilon^2) \tag{8}$$

where the characteristic velocity u_c and p_c are given by

$$u_c = \frac{\Phi}{2h(0)}, \qquad p_c = \frac{\mu \Phi L}{2(h(0))^3} \tag{9}$$

The classical lubrication approximation is obtained from Eqs. (6)–(8) by simply putting the derivative of y_m and h to zero. Hence, in the standard case, the velocities and the pressure depend only on the (half) relative distance h between the walls. Note that the prescribed parabolic inlet velocity profile Eq. (4) is matched in *average* by the second-order approximation. It is matched *exactly* if we have simultaneously $y'_m = h' = 0$ and $y''_m = h'' = 0$. If not, there is a discontinuity and the approximation is correct far enough from the inlet, while near the inlet, there exists a boundary layer that can be determined by a *matched* asymptotic expansion of the governing equations.

3. Asymptotic analysis

3.1. Dimensionless problem and rescaled equations

In order to non-dimensionalize the problem, the following variables are introduced

$$\mathsf{x} = \frac{x}{L}, \qquad \mathsf{u}(\mathsf{x},\mathsf{y}) = \frac{u}{u_c}, \qquad \mathsf{v}(\mathsf{x},\mathsf{y}) = \frac{v}{u_c}, \qquad \mathsf{p}(\mathsf{x},\mathsf{y}) = \frac{p}{p_c} \tag{10}$$

The recentered and rescaled vertical coordinate, defined by Eq. (2), reads now

$$\mathsf{y} = \frac{y - h(0)\mathsf{y}_m(\mathsf{x})}{h(0)\mathsf{h}(\mathsf{x})} \tag{11}$$

where

$$\mathsf{y}_m(\mathsf{x}) = \frac{y_m(L\mathsf{x})}{h(0)}, \qquad \mathsf{h}(\mathsf{x}) = \frac{h(L\mathsf{x})}{h(0)} \tag{12}$$

denote the rescaled shape functions that define the channel's geometry.

Introducing the dimensionless differential operators

$$\hat{\partial}_{\mathsf{x}} = \partial_{\mathsf{x}} - \frac{\mathsf{h}'\mathsf{y} + \mathsf{y}'_m}{\mathsf{h}}\,\partial_{\mathsf{y}}, \qquad \hat{\partial}_{\mathsf{y}} = \frac{1}{\mathsf{h}}\,\partial_{\mathsf{y}}, \qquad \hat{\partial}_{\mathsf{yy}} = \frac{1}{\mathsf{h}^2}\,\partial_{\mathsf{yy}} \tag{13}$$

$$\hat{\partial}_{\mathsf{xx}} = \partial_{\mathsf{xx}} + \frac{\left(\mathsf{h}'\mathsf{y} + \mathsf{y}'_m\right)^2}{\mathsf{h}^2}\,\partial_{\mathsf{yy}} - 2\frac{\mathsf{h}'\mathsf{y} + \mathsf{y}'_m}{\mathsf{h}}\,\partial_{\mathsf{xy}} + \left(\frac{2\mathsf{h}'\left(\mathsf{h}'\mathsf{y} + \mathsf{y}'_m\right)}{\mathsf{h}^2} - \frac{\mathsf{h}''\mathsf{y} + \mathsf{y}''_m}{\mathsf{h}}\right)\partial_{\mathsf{y}} \tag{14}$$

where ∂_{x} and ∂_{y} are the usual derivatives with respect to x and y respectively, the Stokes equations read, in non-dimensional form, as

$$\hat{\partial}_{\mathsf{x}}\mathsf{u} + \frac{1}{\varepsilon}\,\hat{\partial}_{\mathsf{y}}\mathsf{v} = 0 \tag{15}$$

$$\hat{\partial}_{\mathsf{xx}}\mathsf{u} + \frac{1}{\varepsilon^2}\,\hat{\partial}_{\mathsf{yy}}\mathsf{u} = \frac{1}{\varepsilon^2}\,\hat{\partial}_{\mathsf{x}}\mathsf{p} \tag{16}$$

$$\hat{\partial}_{\mathsf{xx}}\mathsf{v} + \frac{1}{\varepsilon^2}\,\hat{\partial}_{\mathsf{yy}}\mathsf{v} = \frac{1}{\varepsilon^3}\,\hat{\partial}_{\mathsf{y}}\mathsf{p} \tag{17}$$

These equations are written in the rescaled region $(0,1)\times(-1,1)$, and are complemented by the boundary conditions

$$\mathsf{u}(0,\mathsf{y}) = \frac{3}{2}\left(1-\mathsf{y}^2\right), \qquad \mathsf{v}(0,\mathsf{y}) = \mathsf{u}(\mathsf{x},\pm 1) = \mathsf{v}(\mathsf{x},\pm 1) = 0, \qquad \mathsf{p}(1,\mathsf{y}) = 0 \tag{18}$$

Next, we follow an asymptotic approach, valid for small ε, in which we assume that the solution $(\mathsf{u},\mathsf{v},\mathsf{p})$ can be expanded in powers of ε, namely

$$\mathsf{u}(\mathsf{x},\mathsf{y}) = \sum_{i=0}^{\infty} \varepsilon^i \mathsf{u}_i(\mathsf{x},\mathsf{y}), \qquad \mathsf{v}(\mathsf{x},\mathsf{y}) = \sum_{i=0}^{\infty} \varepsilon^i \mathsf{v}_i(\mathsf{x},\mathsf{y}), \qquad \mathsf{p}(\mathsf{x},\mathsf{y}) = \sum_{i=0}^{\infty} \varepsilon^i \mathsf{p}_i(\mathsf{x},\mathsf{y}) \tag{19}$$

The fields $(\mathsf{u}_i,\mathsf{v}_i,\mathsf{p}_i)$ will be determined by inserting expressions (19) in Eqs. (15)–(18).

3.2. Correction to CLA in the vertical velocity v_1

To begin with, we shall see that the analysis of the problem at the leading orders provides the standard Reynolds equation within CLA, corrected by a non-vanishing vertical velocity. Introducing expressions (19) in Eqs. (15)–(18), we firstly examine the dominant order terms. The continuity equation (15) reads as $\hat{\partial}_y v_0 = 0$, which leads to

$$v_0 = 0 \tag{20}$$

because of the no-slip conditions $v_0(x, \pm 1) = 0$. The momentum balance along y (17) gives $\hat{\partial}_y p_0 = 0$, so that p_0 is independent of y and we set $p_0 = \bar{p}_0(x)$. The momentum balance along x (16) then reads as $\hat{\partial}_{yy} u_0 = \partial_x \bar{p}_0(x)$, which can be integrated with respect to y using the no-slip boundary conditions $u_0(x, \pm 1) = 0$. This gives the classical parabolic shape for the longitudinal velocity at the dominant order

$$u_0(x, y) = -\frac{h^2}{2} \partial_x \bar{p}_0 (1 - y^2) \tag{21}$$

At the next order, the continuity equation (15) reads as

$$\hat{\partial}_x u_0 + \hat{\partial}_y v_1 = 0 \tag{22}$$

By integrating this equation with respect to y over $(-1, 1)$, we obtain the standard Reynolds equation

$$\partial_x \left(-\frac{2}{3} h^3 \partial_x \bar{p}_0 \right) = 0 \tag{23}$$

where we used the expression of u_0 (21) and the no-slip boundary conditions $v_1(x, \pm 1) = 0$. This shows us that the rescaled flux

$$\phi_0 = -\frac{2}{3} h^3 \partial_x \bar{p}_0 \tag{24}$$

is a quantity conserved along the channel. Comparing the boundary conditions $u_0(0, y) = \frac{3}{2}\left(1 - y^2\right)$ to Eq. (21) provides $\phi_0 = 2$. Finally, the longitudinal velocity at the dominant order reads as

$$u_0(x, y) = \frac{3}{2h} (1 - y^2) \tag{25}$$

The pressure $\bar{p}_0$ in the channel can now be deduced by integration of Eq. (24). Given the boundary condition $p_0(1, y) = 0$, we get

$$p_0(x, y) = \bar{p}_0(x) = \int_x^1 \frac{3}{h^3} \, dx' \tag{26}$$

We are now able to derive the first non-trivial contribution to the vertical velocity. Since u_0 is known from Eq. (25), the continuity equation (22) can be integrated with respect to y, which leads to the first correction to CLA in the vertical velocity

$$v_1(x, y) = \frac{3}{2} \left(1 - y^2\right) \frac{h' y + y'_m}{h} \tag{27}$$

3.3. Extended lubrication approximation and corrections in (u_2, p_2)

We shall now complement the correction in the vertical velocity obtained above by deriving the correction in the pressure and the associated horizontal velocity. To achieve this, we examine the terms of higher orders in Eqs. (15)–(17). Because of $v_0 = 0$, the terms p_1, u_1 and v_2 satisfy the same relations as at lower order, namely

$$\hat{\partial}_x u_1 + \hat{\partial}_y v_2 = 0, \qquad \hat{\partial}_{yy} u_1 = \hat{\partial}_x p_1, \qquad \hat{\partial}_y p_1 = 0 \tag{28}$$

This provides the same result, with $p_1(x, y) = \bar{p}_1(x)$, $u_1(x, y) = \frac{h^2}{2} \partial_x \bar{p}_1 (y^2 - 1)$ and the flux $\phi_1 = -\frac{2}{3} h^3 \partial_x \bar{p}_1$ conserved along x. However, the boundary conditions (18), by means of the prescribed inlet velocity $u_1(x, 0) = 0$ and pressure at the exit $p_1(1, y) = 0$, imply $\phi_1 = 0$ and

$$u_1(x, y) = 0, \qquad p_1(x, y) = 0 \tag{29}$$

Integrating the continuity equation at this order leads to

$$v_2(x,y)=0 \tag{30}$$

The pursuit of the analysis at the next order is necessary to reveal new contributions from Eqs. (15)–(17). Specifically, we now start with

$$\hat{\partial}_x u_2+\hat{\partial}_y v_3=0, \qquad \hat{\partial}_{xx}u_0+\hat{\partial}_{yy}u_2=\hat{\partial}_x p_2, \qquad \hat{\partial}_{yy}v_1=\hat{\partial}_y p_2 \tag{31}$$

Given the non-trivial value (27) of v_1, the pressure p_2 is deduced, up to a constant of x, by integrating the third equation of (31). We obtain

$$p_2(x,y)=\bar{p}_2(x)+\frac{3}{2h^2}\left(h'\left(1-3y^2\right)-2y'_m y\right) \tag{32}$$

where $\bar{p}_2(x)$ is the average of p_2 over $y\in(-1,1)$. The longitudinal velocity u_2 is then calculated thanks to the second equation of (31). Plugging the forms of u_0 and p_2 from Eqs. (25) and (32) into this equation leads to

$$\partial_{yy}u_2=-\frac{3}{h}\left(hh''\left(3y^2-1\right)+2h'^2\left(1-6y^2\right)-2y'^2_m+2\left(hy''_m-6h'y'_m\right)y\right)+h^2\hat{\partial}_x\bar{p}_2 \tag{33}$$

The integration of this expression, taken into account the no-slip conditions $u_2(x,\pm1)=0$, provides u_2 of the form

$$u_2(x,y)=3(1-y^2)\left[\frac{hh''-4h'^2}{4h}y^2-\frac{hh''+y'^2_m}{4h}+\left(\frac{y''_m}{3}-\frac{2h'y'_m}{h}\right)y-\frac{h^2}{6}\hat{\partial}_x\bar{p}_2\right] \tag{34}$$

with $\hat{\partial}_x\bar{p}_2$ still unknown at this stage. In order to determine this term, the first equation of (31) is integrated over $y\in(-1,1)$, which leads to $\int_{-1}^{1}\hat{\partial}_x u_2\,dy=0$ because of the no-slip conditions $v_3(x,\pm1)=0$, and eventually

$$h^3\hat{\partial}_x\bar{p}_2=-\frac{6}{5}\left(hh''+h'^2+5y'^2_m\right) \tag{35}$$

Finally, plugging the above expression into Eq. (34) leaves us with

$$u_2(x,y)=\frac{3}{2h}\left(1-y^2\right)\left(\frac{4h'^2-hh''}{10}\left(1-5y^2\right)+\frac{2hy''_m-12h'y'_m}{3}y\right) \tag{36}$$

The pressure $\bar{p}_2$ is obtained by integrating Eq. (35) with the boundary condition $\bar{p}_2(1)=0$, which gives

$$\bar{p}_2(x)=\int_x^1\frac{6}{5h^3}\left(h'^2+hh''+5y'^2_m\right)\,dx' \tag{37}$$

3.4. Reconstruction of the solution

By adding the contributions at each order (Eqs. (25), (29) and (36) for u; Eqs. (20), (27) and (30) for v; Eqs. (26), (29) and (32) along with (37) for p), we reconstruct an approximation of the solution (u,v,p) up to the second order in ε. In dimensionless form, this gives us

$$u=\frac{3}{2h}(1-y^2)\left[1+\varepsilon^2\left(\frac{4h'^2-hh''}{10}(1-5y^2)+\frac{2hy''_m-12h'y'_m}{3}y\right)\right]+o(\varepsilon^2) \tag{38}$$

$$v=\frac{3\varepsilon}{2h}\left(1-y^2\right)\left(h'y+y'_m\right)+o(\varepsilon^2) \tag{39}$$

$$p=\int_x^1\frac{3}{h^3}\left(1+\frac{2\varepsilon^2}{5}\left(h'^2+hh''+5y'^2_m\right)\right)dx'+\frac{3\varepsilon^2}{2h^2}\left(h'\left(1-3y^2\right)-2y'_m y\right)+o(\varepsilon^2) \tag{40}$$

which, coming back to the dimensional parameters defined by Eq. (10), gives the form announced in Eqs. (6)–(8).

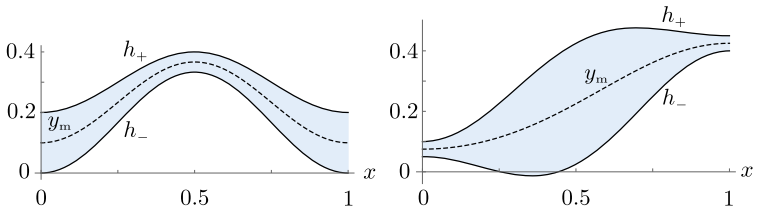

Fig. 2. Profiles used for the comparisons with the full scale simulations: (left) channel's profile (P1), (right) channel's profile (P2).

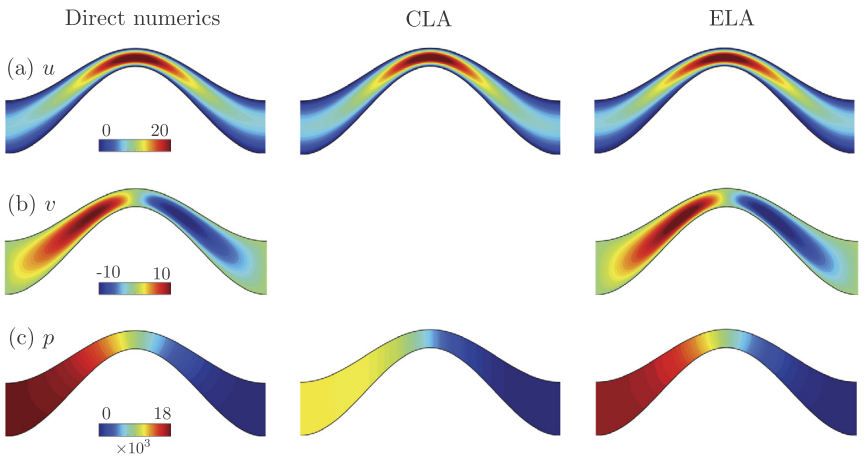

Fig. 3. Results for the profile (P1). Fields of the velocity components (u, v) and of the pressure p in full-scale simulations, CLA and ELA.

Table 1
Typical values of the characteristics of the profiles chosen for the comparison.

Profile	max(2h)	h'	h''	y'_m	y''_m
(P1)	0.2	~ 0.2	~ 1	~ 1	~ 5
(P2)	0.4	~ 0.5	~ 3	~ 0.5	~ 2

4. Validation of the ELA model

To inspect the accuracy of the ELA model specified by Eqs. (6)–(8), we consider two channel profiles (P1) and (P2), where both y_m and h vary. The geometries of the channels, of length $L = 1$, are defined by the following equations:

$$\text{(P1)} \begin{cases} h_+(x) = 0.2\cos(\pi(x-1/2))^2 + 0.2 \\ h_-(x) = \frac{1}{3}\cos(\pi(x-1/2))^2 \end{cases} \tag{41}$$

$$\text{(P2)} \begin{cases} h_+(x) = 0.15\cos(\pi(x-1/2))^2 + 0.1 + 0.35\cos(\pi(x/2-1/2))^2) \\ h_-(x) = -0.2\cos(\pi(x-1/2))^2 + 0.05 + 0.35\cos(\pi(x/2-1/2))^2 \end{cases} \tag{42}$$

These profiles are represented in Fig. 2. For (P1) and (P2), we have $h'_+(0) = h'_-(0) = 0$ and $h'_+(1) = h'_-(1) = 0$. The prescribed inlet velocity (4) is chosen such that the flux is $\Phi = 1$ and the fluid viscosity is set at $\mu = 1$. We use COMSOL to solve the direct problem (3) along with the boundary conditions (4).

We report in Figs. 3, 4, and 5 the fields of the velocity components (u, v) and of the pressure p computed numerically and the corresponding fields predicted by the CLA and ELA; for the CLA, $v(x, y) = 0$ is not shown.

In the reported cases, the profiles have the characteristics given in Table 1. The two channels have a reasonable small slenderness ratio max(2h) as well as moderate slopes/curvatures, which do not exceed a few unities. Besides they produce flows with similar maximum horizontal velocities and similar pressure drops. However, the improvement of ELA compared to CLA is much more impressive for (P1) than for (P2) and we shall see that this is attributable to more significant slopes y'_m of the centerline, a parameter that is not related to the slenderness ratio. Hence, even though (P1) has a smaller slenderness ratio, the deviation of the flow characteristics with respect to the CLA prediction is more significant, and interestingly, the asymptotic analysis appears to be more robust with respect to large centerline slopes than to large slenderness ratios.

To begin with, it is noticeable that CLA and ELA have the same good accuracy to capture the right variations of $u(x, y)$ and this is expected since the correction δu of ELA appears at the second order. From Eq. (6), this correction near the

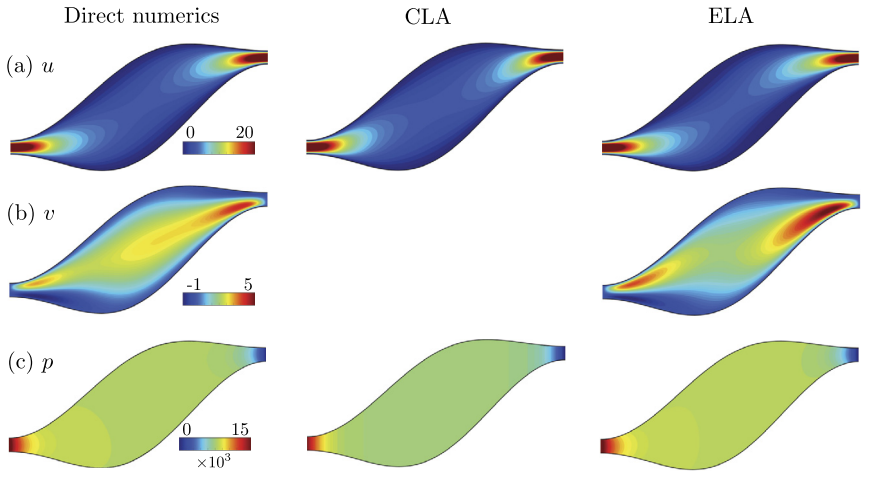

Fig. 4. Results for the profile (P2). Same representation as in Fig. 3.

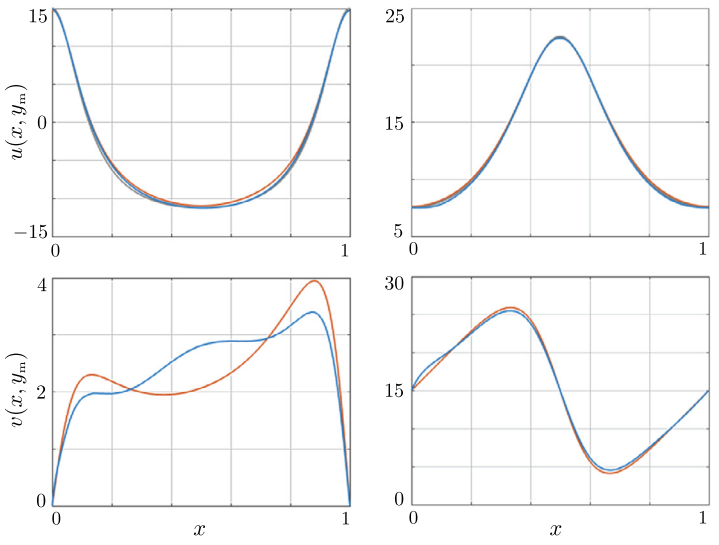

Fig. 5. Variations of the horizontal velocity $u(x, y_m)$ and vertical velocity $v(x, y_m)$ with respect to x, calculated at the centerline $y = y_m$. The red line shows the velocity field computed numerically, the blue line shows the prediction in ELA from (8); the grey line shows the horizontal velocity in CLA (we do not represent the vertical velocity as it is neglected in CLA).

centerline varies as $\delta u \sim (4h'^2 - hh'')/10 \sim 0.01$ in the reported cases. Accordingly, we find an error averaged on the whole channel of about 2% for (P1) and 4% for (P2). The effect on the vertical velocity $v(x, y)$ is much more significative and again this is expected since the correction appears at the first order. But in this case, from Eq. (7), v is crucially dependent on y'_m, since $v/u \sim y'_m$ near the centerline. It results that the large slope of the mean line in (P1) close to unity produces vertical velocities up to half the horizontal one.

We now move on to the fields of pressure, which are of particular interest since the pressure drop due to expansions/constrictions are important in many practical situations. As for the vertical velocity, the gain in the ELA is more impressive for (P1) than for (P2), although the slenderness ratio of the former is half that of the latter: for (P1), the error between the prediction and the direct numerics is of about 5% for ELA, while this error is of about 40% for CLA; for (P2) the error is of 1% for ELA versus 10% for CLA. To better understand the influence of the different parameters in the ELA, we define $p_{CLA}(x) = \mu\Phi \int_x^L 3/(2h^3)\,dx'$ as the pressure predicted by the CLA; from Eq. (8), the ELA involves two corrections compared to the CLA

$$p(x, y) = p_{CLA}(x) + \delta\bar{p}(x) + \delta p(x, y) \tag{43}$$

with

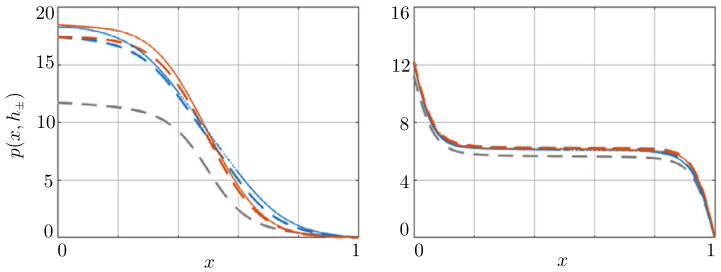

Fig. 6. Variations of the pressure with respect to x. Plain lines show the pressure profiles $p(x,h_\pm)$ computed numerically (blue at $y=h_+$, red at $y=h_-$), dotted lines show the prediction in ELA from (8); dashed grey lines show $p(x,y)=p_{\mathrm{CLA}}(x)$ being independent of y in CLA.

$$\delta\bar{p}=\mu\Phi\int_x^L\frac{3}{5h^3}\left(h'^2+hh''+5y'^2_{\mathrm{m}}\right)\mathrm{d}x',\qquad \delta p=\frac{3\mu\Phi}{4h^2}\left(h'(1-3\mathrm{y}^2)-2y'_{\mathrm{m}}\mathrm{y}\right)$$

The term δp tells us that the isolines of pressure are not vertical and its relative weight $\delta p/p_{\mathrm{CLA}}\sim hh'/L$ is given by the slenderness ratio, hence here negligible. Conversely, the term $\delta\bar{p}$ is an integral along x (as p_{CLA}) and as such it cumulates the effects of slopes and curvatures. Its weight contains a contribution in $\int y'^2_{\mathrm{m}}/h^3$, which becomes significant when large variations of the centerline coincide with small slenderness. This happens for (P1) but not for (P2) and the consequences are shown in Fig. 6, where we reported the pressure profiles $p(x,h_\pm)$ along the channel walls computed numerically, and the CLA and ELA predictions. For (P1), the actual pressure drop, $\bar{p}(0)\sim 18{\cdot}10^3$, is correctly predicted by ELA while largely underestimated by CLA. In contrast, the gain for (P2) in ELA is moderate compared to CLA.

5. Conclusion

We have derived in this paper a second-order lubrication approximation for a viscous flow at low Reynolds number in thin channels with arbitrary walls shape. Velocity and pressure profiles in the channel have been given as fully explicit functions of the inlet flux and the walls geometry, up to the second derivative. The resulting ELA is in general better than the CLA and this has been exemplified by comparison with direct numerics. However, there are situations where the CLA fails in accurate predictions, although the criterion of small slenderness ratio is met. These situations correspond to channels containing constrictions coinciding with large variations of the centerline. This results in large vertical velocities and pressure drops largely underestimated by CLA and accurately reproduced by ELA.

Extension of the current work deals with the derivation of a similar higher-order lubrication approximation for (i) moderate (yet non-negligible) Reynolds numbers, starting from the full Navier–Stokes equation, (ii) non-stationary case with time-varying walls.

References

[1] O. Reynolds, On the theory of lubrication and its application to mr. Beauchamp tower's experiments, including an experimental determination of the viscosity of olive oil, Philos. Trans. R. Soc. Lond. 177 (1886) 157–234.
[2] B.J. Hamrock, S.R. Schmid, B.O. Jacobson, Fundamentals of Fluid Film Lubrication, CRC Press, Boca Raton, FL, USA, 2004.
[3] E. Detournay, Propagation regimes of fluid-driven fractures in impermeable rocks, Int. J. Geomech. 4 (2004) 35–45.
[4] B. Taisne, S. Tait, C. Jaupart, Conditions for the arrest of a vertical propagating dyke, Bull. Volcanol. 73 (2011) 191–204.
[5] J.R. Lister, Buoyancy-driven fluid fracture: similarity solutions for the horizontal and vertical propagation of fluid-filled cracks, J. Fluid Mech. 217 (1990) 213–239.
[6] Y. Aboelkassem, A. Staples, A bioinspired pumping model for flow in a microtube with rhythmic wall contractions, J. Fluids Struct. 42 (2013) 187–204.
[7] E. Hasegawa, H. Izuchi, On steady flow through a channel consisting of an uneven wall and a plane wall: Part 1. Case of no relative motion in two walls, Bull. JSME 26 (1983) 514–520.
[8] M. Van Dyke, Slow Variations in Continuum Mechanics, Advances in Applied Mechanics, vol. 25, Elsevier, 1987, pp. 1–45.
[9] S. Sisavath, A. Al-Yaarubi, C.C. Pain, R.W. Zimmerman, A simple model for deviations from the cubic law for a fracture undergoing dilation or closure, in: Thermo-Hydro-Mechanical Coupling in Fractured Rock, Springer, 2003, pp. 1009–1022.
[10] J. Fabricius, Y. Koroleva, A. Tsandzana, P. Wall, Asymptotic behaviour of Stokes flow in a thin domain with a moving rough boundary, Proc. R. Soc. A 470 (2014) 20130735.
[11] B. Tavakol, G. Froehlicher, D.P. Holmes, H.A. Stone, Extended lubrication theory: improved estimates of flow in channels with variable geometry, Proc. R. Soc. A 473 (2017) 20170234.